Synchrotron-radiation photoemission spectroscopy of octahedrally coordinated layer compounds

G. Margaritondo* and J. E. Rowe
Bell Laboratories, Murray Hill, New Jersey 07974
(Received 17 October 1978)

The polarized uv continuum emitted by the University of Wisconsin Storage Ring has been employed to study the electronic structure of SnS_2, PbI_2, and BiI_3 with several different photoemission-spectroscopy techniques. For binding energy ~ 11.5 eV with respect to the top of the valence band, E_v, four valence-band density-of-states peaks have been found for SnS_2 and five each for PbI_2 and BiI_3. In the energy region extending from the vacuum level to ~ 14 eV above it the photoelectron spectra exhibit six conduction-band density-of-states peaks for SnS_2 and PbI_2 and four for BiI_3. A theoretical analysis of the results shows that in all three materials the anion p states give the main contribution to the valence band and the cation p states to the bottom of the conduction band. The transfer of electrons from cation p states to anion p states leaves two filled s states in each cation which also contribute to the valence-band spectrum. For SnS_2 these states have been found ~ 7.4 eV below E_v, while for PbI_2 and BiI_3 they combine to some extent with anion $(s\text{-}p)$ hybrid orbitals, giving a shallow occupied state with antibonding character as well as a bonding state deep in the valence band. More details about the wave-function symmetry have been provided by photon-polarization effects and by spectra taken in a normal-emission geometry. Little dispersion of the normal emission energy-distribution-curves peaks with respect to photon energy variation was observed, and this indicates that the interlayer interactions are weaker here than in the tetrahedrally coordinated III-VI compounds.

I. INTRODUCTION

The band structure of three layer compounds with octahedral coordination of the anions around each cation, SnS_2, PbI_2, and BiI_3, has been investigated with several different synchrotron-radiation uv photoemission-spectroscopy (UPS) techniques. The investigation has been carried out over an energy range extending below and above the Fermi level E_F. The experimental method[1] consisted of taking energy distribution curves (EDC's) and constant initial-state (CIS) curves[2] for different photon polarization, therefore exploiting continuity and polarization, two of the most important features of synchrotron radiation. The power of this approach has been established by recent experiments on III-VI compounds.[1] Most of the EDC features are related to peaks of the valence-band density of states. Comparing EDC's taken at different photon energies allows one to separate density-of-states effects from matrix-element and final-state effects. Photon polarization effects on the EDC's provide information on the symmetry of the initial-state wave function. Information on the *conduction*-band density of states is provided by the CIS curves after a detailed analysis and elimination of spurious contributions such as two-step direct recombination photoionization effects.[2-4] In summary, this experimental method provides a rather complete picture of the density of states over a wide energy region. In the present case the method has been completely successful in studying the electronic structure of SnS_2, PbI_2, and BiI_3. Even more band-structure information has been obtained than for III-VI compounds,[1] since an angle-resolved photoelectron collection geometry has been employed in this work as well as the angle-integrated geometry of Ref. 1.

The choice of SnS_2, PbI_2, and BiI_3 for the present investigation was influenced by many factors. They are layer compounds with nonreactive surfaces. Thus they share with the III-VI's good characteristics such as cleanliness, even under moderate vacuum conditions, and a marked two-dimensional character which simplifies their theoretical treatment.[5-10] Their structures have some similarity with that of GaSe, which makes it interesting to compare the respective UPS results. The main difference between the two structures is the presence in the GaSe-like crystals of cation-cation bonds normal to the layer which are not found in SnS_2, PbI_2, and BiI_3. The present results confirm that the cation-cation bonds are related to the strong photon polarization effects found in the EDC's of GaSe, GaS, and InSe[1,11] and that they play a critical role in determining the electronic structure of these crystals.

This paper will be structured as follows. Section II will describe the experimental procedure and the results. Sections III, IV, and V will discuss the results for SnS_2, PbI_2, and BiI_3, respectively. A summary of the most important conclusions will be reported in Sec. VI.

II. EXPERIMENTAL PROCEDURE AND RESULTS

The experiments have been carried out at the University of Wisconsin Storage Ring using a beam line equipped with a bakable vertical Seya-Namioka monochromator.[12] The experimental chamber had a base vacuum $<1.5\times10^{-10}$ Torr, although the low chemical reactivity of these samples has allowed taking data at pressures in the 10^{-9}-Torr range. All the data have been taken on samples freshly cleaved *in situ*, whose cleanliness has been verified by means of Auger-electron spectroscopy.[13] The photoelectron energy E has been analyzed with a double-pass PHI cylindrical mirror analyzer (CMA). The monochromator and the CMA have been driven in parallel by a PDP $8/L$ minicomputer programmed to take UPS curves in several different modes. In particular, EDC's have been taken keeping the photon energy $\hbar\omega$ constant and sweeping E, while CIS curves have been taken sweeping both $\hbar\omega$ and E and keeping the difference $E-\hbar\omega=E_i$ constant. The entire experimental chamber could be rotated under ultrahigh vacuum conditions around the beam line as described in Ref. 1. The rotation allowed changing the photon polarization from p to s and vice versa without changing either the angle-integrated photoelectron collection geometry or the direction of incidence of the photons. In particular, the geometry for s polarization corresponded to a zero component of the photon electric field perpendicular to the sample, i.e., $E_z=0$. Most of the data have been taken in an angle-integrated collection geometry, but for some of the spectra a shield with a hole has been placed in front of the CMA so that only photoelectrons emitted within a small solid angle were accepted. The latter geometry has been employed to select photoelectrons emitted within ~5° from the normal to the sample surface.

It is known that most structures in the UPS curves at low photon energy, $\hbar\omega<30$ eV, are related to critical points in the joint density of states, i.e., $\nabla_k(E_i-E_f)=0$, where E_i = initial-state energy and E_f = final-state energy. For

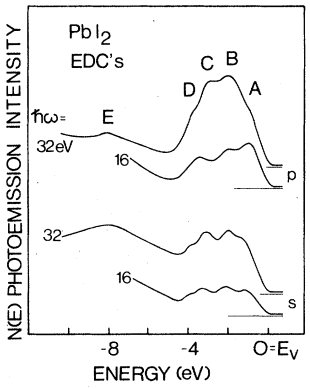

FIG. 2. Angle-integrated EDC's for PbI_2.

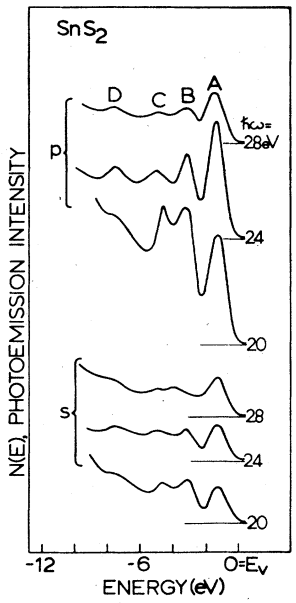

FIG. 1. EDC's taken on SnS_2 at several photon polarizations. An angle-integrated photoelectron collection geometry has been employed here and the curves have been normalized in intensity to the same uv photon flux. with a flat spectral photon energy distribution.

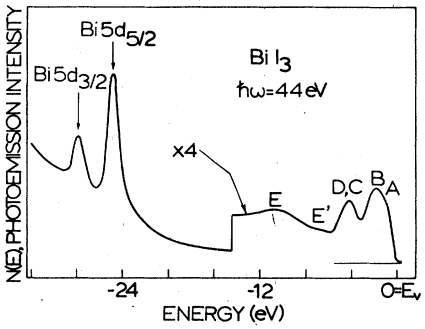

FIG. 3. Angle-integrated BiI_3 EDC's at $\hbar\omega=44$ eV and p polarization. The energy range has been extended to include the Bi $5d$ spin-orbit doublet.

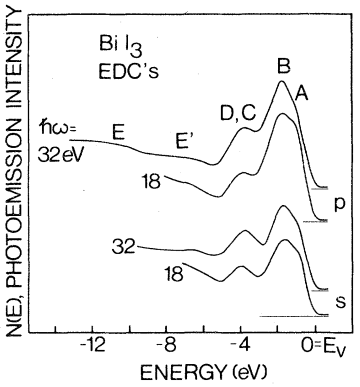

FIG. 4. Angle-integrated EDC's for BiI_3.

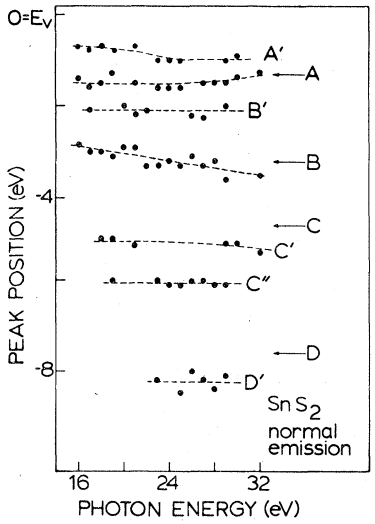

FIG. 6. Energy position of the normal-emission SnS_2 EDC peaks of Fig. 5 the photon energy. The positions of the angle integrated peaks C and D not appearing in the normal-emission EDC's are shown for comparison.

EDC's in the high-photon-energy limit this condition practically reduces to $\nabla_k E_i = 0$, i.e., in that case the EDC peaks coincide with maxima of the *initial* density of states. At low photon energies final-state contributions and matrix-element effects produce excursions of the EDC peaks around their high-photon-energy positions. Comparing EDC's taken at small and large photon energies usually allows separation of these effects from the initial-state contributions, and the energy position of the valence-band density-of-states structure can be carefully determined in this way. It is convenient to take CIS curves selecting the constant $E_i = E - \hbar\omega$ to coincide with one of the critical point maxima in the valence-band density of states

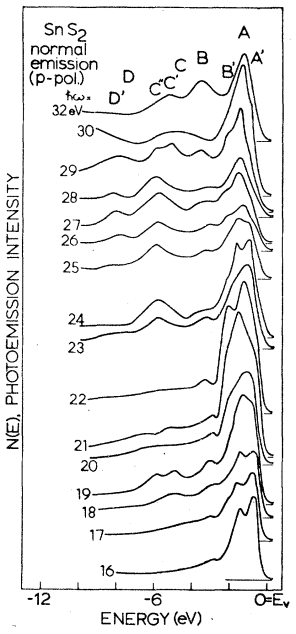

FIG. 5. Normal-emission SnS_2 EDC's taken with p-polarized photons of several different energies.

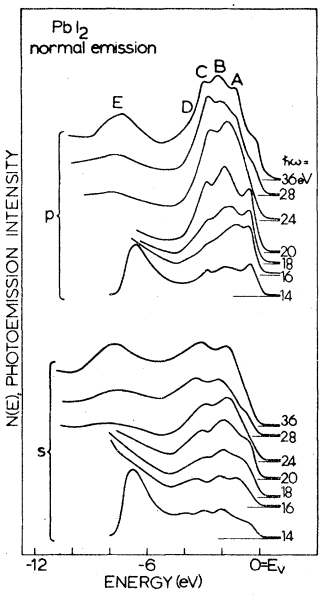

FIG. 7. Normal-emission EDC's for PbI_2 taken with p- and s-polarized photons of several different energies.

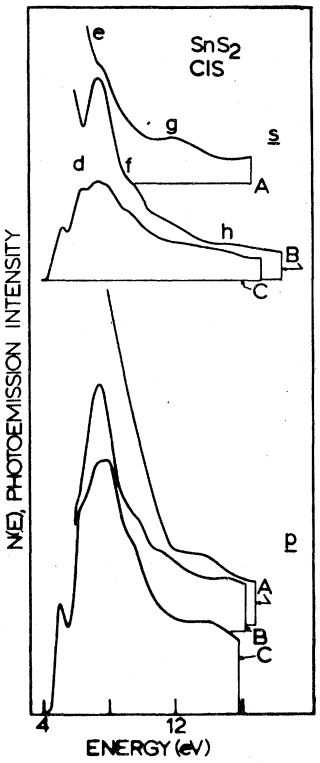

FIG. 8. Angle-integrated SnS_2 CIS curves as a function of final-state energy. The capital letter at the right side of each curve indicates the valence-band peak whose position in energy coincides with the value of the constant $E_i = E_f - \hbar\omega$, i.e., the initial-state energy for primary photoionization contributions to the same CIS curve.

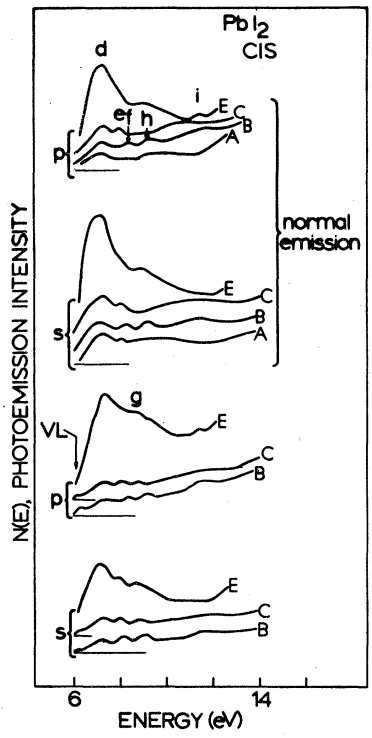

FIG. 9. Angle-integrated and normal-emission PbI_2 CIS curves as a function of final-state energy.

experimentally deduced from the EDC's. Since E_i corresponds to an initial-state critical point, one has $\nabla_k E_i = 0$, and the condition $\nabla_k (E_i - E_f) = 0$ reduces to $\nabla_k E_f = 0$. Thus peaks in the CIS curves taken in this way should coincide with critical points in the final density of states. Of course, the present analysis only applies to first-order photoionization processes, while two-step direct recombination processes can give spurious CIS peaks.[3,4] The CIS peaks due to maxima in the final density of states can be easily recognized while comparing CIS curves taken for different critical-point values of the initial energy E_i. Indeed, these peaks must appear in different curves at the same values of E_f, which is the final-state energy for primary photoionization processes.

Typical angle-integrated EDC's are shown in Fig. 1 for SnS_2, in Fig. 2 for PbI_2, and in Figs. 3 and 4 for BiI_3. Four structures are observed

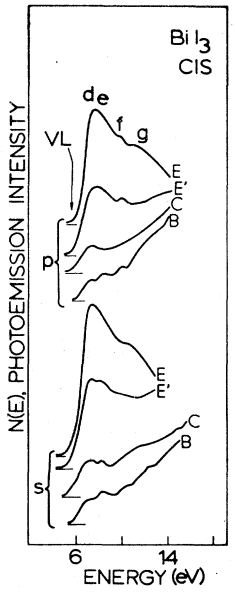

FIG. 10. Angle-integrated BiI_3 CIS curves as a function of final-state energy.

TABLE I. Energy positions of the SnS_2 EDC peaks (capital letters) and CIS peaks (small letters).[a]

Peak[b]	Experimental position[c] (eV)	Theoretical position[d] (eV)	Character[d]
Sn4$d_{3/2}$	−25.1 ±0.2		
Sn4$d_{5/2}$	−24.1 ±0.2		
D′	− 8.2 ±0.4	− 6.0	Sn(*s*)
D	− 7.4 ±0.2		
C″	− 5.5 ±0.3		S(*s*)
C′	− 4.8 ±0.3	− 4.9	
C	− 4.6 ±0.4		
B	− 3.2 ±0.4	− 3.1, − 2.8	
B′	− 2.1 ±0.3		
A	− 1.3 ±0.3	− 1.0	
A′	− 0.8 ±0.3		
Vacuum level	4.8 ±0.3	5.1	
...	5.1 ±0.2	5.4	Sn(*s*) + some *d* character not as well defined as for peaks *d* & *e*
d	6.25±0.2	6.8	
e	7.4 ±0.3	7.7	
f	9.5 ±0.3	9.6, 8.6	
g	11.45±0.4	11.0	
h	14.0 ±0.3	14.4, 13.3	

[a] Energies measured from E_V.
[b] Peaks *D′*, *C″*, *C′*, *B′* and *A′* only appear in normal-emission EDC's.
[c] Uncertainties larger than 0.2 eV reflect large $\hbar\omega$ dispersion.
[d] Reference 6.

TABLE II. Energy positions of the PbI_2 photoemission spectral peaks.[a]

Peak	Experimental position	Theoretical position[b]	Character[b]
Pb5$d_{3/2}$	−20.8 ± 0.2		
Pb5$d_{5/2}$	−18.8 ± 0.2		
F	−12.2 ± 0.4[c]	−11.5	I(*s*)
E	− 8.2 ± 0.3	− 5.5	Pb(*s*) + I(sp^3)
D	− 3.8 ± 0.3	− 3.5	
C	− 3.2 ± 0.4	− 3.0	I(*p*)
B	− 2.0 ± 0.3	− 2.0	
A	− 0.8 ± 0.4[d]	− 0.5	Pb(*s*) + I(sp^3)
Vacuum level	6.0 ± 0.2		
d	7.2 ± 0.3		
e	7.8 ± 0.3		
f	8.4 ± 0.2		
g	8.7 ± 0.3		
h	9.2 ± 0.3		
i	11.4 ± 0.3		

[a] See the footnotes to Table II.
[b] References 10 and 17.
[c] X-ray photoemission data from Ref. 17.
[d] Peak A splits in two components separated by ~0.8 eV for *p*-polarization, normal-emission EDC's at $\hbar\omega \geq 28$ eV.

TABLE III. Energy positions of the BiI_3 photoemission spectral peaks.[a]

Peak	Experimental position[b]	Theoretical position[b]	
Bi5$d_{3/2}$	−27.7±0.2		
Bi5$d_{5/2}$	−24.7±0.2		
F	−12.3±0.3[c]	−11.0	I(*s*)
E	−10.8±0.4	− 7.5	Bi(*s*) + I(sp^3)
E'	− 6.6±0.4		
D, *C*	− 3.8±0.3	− 4.0	I(*p*)
B	− 1.8±0.3	− 2.4	
A	− 1.0±0.3	− 0.5	Bi(*s*) + I(sp^3)
Vacuum level	5.6±0.2		
d	7.4±0.3		
e	8.2±0.3		
f	10.0±0.2		
g	11.8±0.5		

[a]See the footnotes to Table I.
[b]References 10 and 17.
[c]X-ray photoemission data from Ref. 17.

for SnS_2 and five each for PbI_2 and BiI_3. These peaks have been labeled with capital letters following the convention of Ref. 1. The angle-resolved EDC's for SnS_2 taken in a direction normal to the sample surface reveal five more structures, *A'*, *B'*, *C'*, *C''*, and *D'* (see Fig. 5), whose energy position does not coincide with any of the peaks of Fig. 1. Figure 6 shows that none of the normal-emission peaks exhibit a strong dispersion versus $\hbar\omega$ except, perhaps, peak *B*. The peaks appearing in the normal-emission PbI_2 EDC's of Fig. 7 essentially coincide with those of Fig. 2, except for a splitting of peak *A* in two components for *p* polarization and $\hbar\omega \gtrsim 28$ eV.

Figure 8 shows angle-integrated SnS_2 CIS curves taken for three different values of initial energy E_i corresponding to the positions of the SnS_2 EDC peaks *A*, *B*, and *C*. Six final-state structures appear in these spectra above the vacuum level (VL), which is the lower limit of the energy region that can be explored by the CIS technique. Again following the conventions of Ref. 1, five of these structures have been labeled as *d*–*h*. No label has been given to the first peak ~5.1 eV above the top of the valence band, E_v, since this peak is spurious due to the onset of photoemission. Figure 9 shows angle-integrated and normal-emission CIS curves for PbI_2 which exhibit six final-state structures labeled *d*–*h*. Only four peaks (*d*–*g*) appear for BiI_3 in the angle-integrated CIS curves of Fig. 10.

The peak positions for the SnS_2 EDC's and CIS curves have been summarized in Table I. The theoretical estimates of these positions are also reported and will be discussed in Sec. III. Similarly, Tables II and III summarize the peak positions for PbI_2 and BiI_3, respectively. We would like to emphasize the wide extent of the energy region covered. The present experimental approach explores a spectral region ~40 eV wide for SnS_2 and BiI_3 and ~32 eV wide for PbI_2. This region extends in the conduction band up to 11–14 eV above the vacuum level. Structure can be found in the conduction-band density of states even at those high energies. Thus rather than being free-electron-like, the conduction bands of these materials exhibit a molecular character much like that of the III-VI compounds.

III. DISCUSSION OF RESULTS FOR TIN DIN-SULFICE

A single crystal of SnS_2, PbI_2, or BiI_3 consists of two-dimensionally extended sandwiches of atoms stacked on top of each other and held together by relatively weak interactions. We shall see that the interlayer interactions appear weaker in these compounds than in the III-VI compounds. Each sandwich is formed by three atomic planes with two anion planes (S or I atoms) in the outside of the layer and one cation plane (Sn, Pb, or Bi atoms) in the inside. Each cation is octahedrally

surrounded by and chemically bound to six anions. For SnS_2 and PbI_2 each anion is chemically bound to three different cations, leading to the CdI_2 lattice structure, whose top view can be seen in Fig. 11(a). One should observe that this lattice structure can be obtained from the GaSe-like structure after removing one of the two cation planes (and the corresponding cation-cation bonds) and rotating one of the anion planes by 60°.

The Sn-S bond length in SnS_2, 2.57 Å, is much closer to the sum of the Sn and S ionic radii, 2.55 Å, than to the sum of the covalent radii. Thus a predominately ionic character of this bond is expected. Charge-density calculations[10] show that the valence-band charge is mostly centered around the sulphur sites. The charge distribution is, however, quite asymmetric around each anion site, and this indicates that some covalent character is also present in the Sn-S bond. In practice, the valence band is mostly formed by filled S($3p$) states with a minor Sn ($5s$)-like contribution.[14] The cation $5p$ states can be found as empty states in the conduction band.[4]

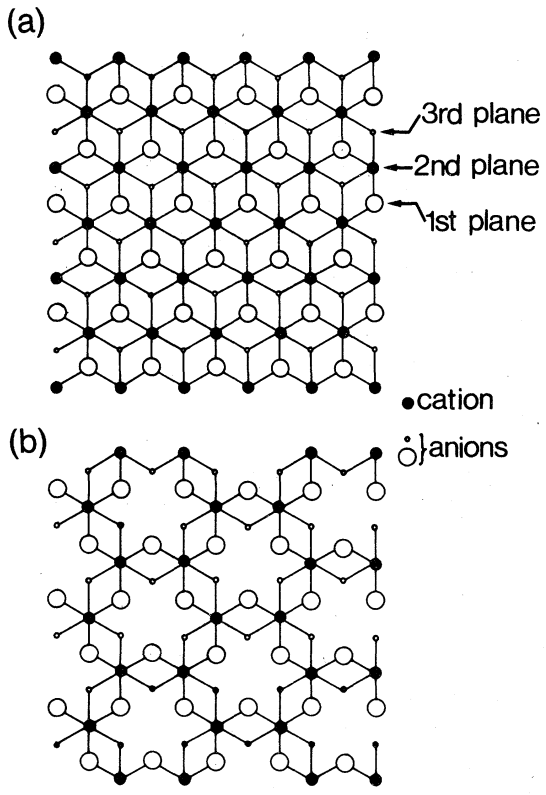

FIG. 11. (a) Top view of the CdI_2-like lattice structure of SnS_2 and PbI_2. Only one layer is shown here and the large and small open circles correspond to its top and bottom atomic planes, respectively. (b) Top view of the BiI_3 lattice structure. Note that here only $\frac{2}{3}$ of the cation sites of the above CdI_2 structure are occupied.

The theoretical valence-band density of states by Schluter *et al.*[6,10] exhibits four peaks, 1.0, 2.8, 4.9, and 6.0 eV below E_v, plus a shoulder at ~ 3.1 eV. These have sulphur p-like character. The angle-integrated EDC peaks A and C must be identified with the theoretical structure at −1.0 and −4.9 eV, respectively. Peak B is a superposition of the two theoretical structures at −2.8 and −3.1 eV. Figures 5 and 6 show that in a normal-emission geometry peaks A and B are accompanied by satellites, peak A' and peak B', respectively. Due to E vs k dispersion, peak c is shifted in the normal-emission EDC's of Fig. 5 from its angle-integrated energy position, giving rise to peak c^1. Similar to peaks A and B, peak c^1 is accompanied by a satellite, peak c^{11}. The normal-emission satellites of peaks A, B, and C originate from a partial removal of the degeneracy between sulphur p_z and p_x, p_y states by crystal-field splitting. A *complete* removal of this degeneracy can be excluded, since it would correspond to strong photon polarization effects on the relative intensity of the EDC structures[1] which have not been observed for SnS_2. A *partial* crystal-field splitting between p_z and p_x, p_y states is supported by previous optical[14] and photoemission[6] data. The normal-emission geometry emphasizes the p_z-like contributions to the p-polarization EDC's,[15] and therefore the normal-emission satellites of peaks A, B, and C have p_z character. Thus the p_z-like components of peaks A, B, and C appear displaced in energy with respect to the remaining components of these peaks, i.e., there is some p_z–p_x, p_y splitting.

The cation s states whose theoretical energy position[10] is 6.0 eV below E_v must be identified with peak D in the angle-integrated EDC's. There is a large discrepancy between theory and experiment as to the postion in energy of these states. We shall see later that similar discrepancies are found for the deep-lying cation s-like contributions to the valence-band density of states of PbI_2 and BiI_2. In the normal-emission EDC's of Fig. 5 peak D is replaced by peak D', and this corresponds, as for peak C, to a shift of peak D from its angle-integrated energy postion due to E vs k dispersion.

A remarkable feature of Figs. 5 and 6 is the absence of strong $\hbar\omega$ -dispersion for many of the normal-emission SnS_2 EDC peaks. The k-vector component perpendicular to the sample surface, $K_\perp$, is not a good quantum number in the photoemission process, and it is difficult to establish a quantitative relationship between the $\hbar\omega$ -dispersion of the normal-emission EDC peaks and

the band structure. Nevertheless, qualitative conclusions can be drawn. In particular, the weak $\hbar\omega$ -dispersion of the normal-emission EDC peaks clearly shows that the interlayer interactions in SnS_2 are weak. Much stronger dispersion of normal photoemission and stronger interlayer interactions have been found for III-VI compounds.[16]

The calculated conduction-band density-of-states peaks by Schluter[6] coincide well with the experimental CIS structures of Fig. 8 so that a straightforward identification of these structures can be attempted. The identification is reported in Table I, which summarizes the theoretical atomic-orbital character of each peak besides its theoretical and experimental positions in energy. One should observe, however, that only peaks d and e exhibit a pronounced atomic character, i.e., Sn-5p character (with minor d-like contributions). The other peaks correspond to more delocalized charge distributions and the atomic-orbital character reported for them in Table I is very weak. This explains in part why photon polarization effects in the CIS curves are weak for SnS_2. Indeed, strong polarization effects mostly depend on the validity of the atomic dipole selection rules and therefore on a marked atomic character of the states involved in the optical transitions.

IV. DISCUSSION OF RESULTS FOR LEAD IODIDE

The single crystals of PbI_2 have the same CdI_2 lattice structure as SnS_2 shown in Fig. 11(a). Contrary to the case of SnS_2, the valence-band charge in PbI_2 has an almost symmetric distribution around the anions[10] so that the Pb-I chemical bond in PbI_2 appears more ionic in character than the Sn-S bond in SnS_2. Therefore, most of the valence-band electrons have I(s) or I(p) character with the former confined lower energies than the latter.[17] Some Pb cation s-like contribution is again present in the valence band but it is not confined to low energies as in SnS_2. The Pb-I bond is established transferring electrons from each lead atom. The Pb(6s) states combine to some extent with iodine valence orbitals. The admixture between Pb(6s) and I(sp^3) gives a pair of hybridized states whose theoretical positions are 5.5 and 0.5 eV below E_v. Therefore, these hybrids, which from the point of view of the total cohesive energy have nonbonding character, appear in the energy spectrum as a bonding-antibonding pair.[10,17]

As it is shown in Table II, peaks B, C, and D correspond to the theoretical peaks with I(5p) character. The aforementioned pair of hybridized Pb(s)+ I(sp^3) states correspond to peaks A and E. The anion 5s electrons give rise to peak F at −12.2 eV, which is much more evident in the x-ray photoemission experiments[17] than in the UPS curves. The normal-emission EDC's of Fig. 7 do not have satellites of the angle-integrated peaks, and this shows that in PbI_2 the degeneracy between anion p_z and p_x, p_y states has not been removed by crystal-field splitting. As for SnS_2, the $\hbar\omega$ -dispersion of the peaks in Fig. 7 is quite small and the interlayer interactions appear weak. A remarkable feature of the normal-emission PbI_2 EDC's is the splitting of peak A in two different peaks separated by~0.8 eV occurring for p -polarization at high photon energies. Since the p_z-like contributions to the EDC's are emphasized for p polarization in a normal-emission geometry,[15] this splitting is explained by an asymmetric distribution of the p_z-like components in the antibonding Pb(s)+ I(sp^2) state. An asymmetric distribution of p_z states seems also present in the *bonding* Pb(s)+ I(sp^3) orbitals, and it produces the asymmetric shape of peak E in the high-photon-energy p polarization EDC's of Fig. 7.

A theoretical analysis of the PbI_2 conduction-band orbital character has been performed for states below the vacuum level VL.[4,10] In this energy region the theoretical PbI_2 conduction band exhibits a strong lead p character. This has been confirmed by recent experimental results[4] on optical transitions from the Pb 5d core level doublet to the bottom of the conduction band which are affected by large excitonic effects. These transitions have quasiatomic character, and their one-electron final states correspond to the Pb(6p) spin-orbit doublet with components ~3.4 and ~4.6 eV above E_v. Some insight into the higher-lying conduction-band states is provided by the analysis of the PbI_2 band structure described in Ref. 7. Peak d originates from the flat portion of the 9th, 10th, 11th, and 12th conduction bands in the region of the Γ point whose theoretical position is ~7 eV above E_v. Peaks e, f, and g are related to the 6th–11th conduction bands near the M point and/or the K point which correspond to maxima in the theoretical density of states 8–8.5 eV above E_v. Also the M-point region is probably responsible for peak h, since there the flat region of the 10th and 11th conduction bands corresponds to maxima in the theoretical density of states ~9 eV above E_v. Peak i corresponds to the theoretical Γ and M points of the 15th and 16th conduction bands which can be found ~11.5 eV above E_v in Ref. 7. The lack of strong photon polarization effects in the CIS curves of PbI_2 indicates that, as in SnS_2, a strong atomic-orbital character is only present in the lower part of the conduction band. Quite probably, the conduction-band peaks

listed in Table I have no unique character, and determining their atomic decomposition would require an extremely careful examination of the corresponding pseudo-charge distributions.

V. DISCUSSION OF RESULTS FOR BISMUTH IODIDE

In the BiI_3 lattice structure each cation is octahedrally surrounded by six anions as in the CdI_2-like structure of SnS_2 and PbI_2. However, the bismuth atoms occupy only $\frac{2}{3}$ of the CdI_2 cation sites, and each anion is chemically bound to *two* rather than to three cations. A top view of the resulting structure can be seen in Fig. 11(b).

As for PbI_2 and SnS_2, the cation-anion bond length of BiI_3, 3.04 Å, compares more favorably with the sum of the ionic radii, 3.20 Å, than with the sum of the covalent radii, 2.79 Å.[10] The theoretical valence-band charge distribution is more symmetric than in SnS_2 but less than in PbI_2 around the anion sites. Thus the cation-anion bond in BiI_3 has an ionicity intermediate between SnS_2 and PbI_2. The mechanism by which the chemical bonds are established is similar to that of PbI_2. There is a transfer of electrons from the bismuth atoms to the iodine atoms and a large contribution of filled iodine p states to the upper part of the valence band. Filled nonbonding s states are left in the bismuth atoms, and these states combine with anion sp^3 hybrids giving a pair of bonding, antibonding valence-band states. Therefore, in spite of the difference in structure the energy distribution of the valence-band states is rather similar in PbI_2 and BiI_3. The distribution consists of a group of anion p-like states 1.5–4 eV below E_v, surrounded by a pair of bonding, antibonding hybridized Bi(s)+ I(sp^3) states.

The experimental results of Figs. 3 and 4 show two peaks, B and C, D, that originate from iodine p orbitals. The XPS data of Ref. 17 suggest indeed that the PbI_2 states C and D merge in BiI_3 into only one peak. Peaks A and E are the bonding and antibonding components of the Bi(s)+ I(sp^3) pair. Again, the experimental binding energy of the deeper valence-band states with contributions from cation s orbitals is much larger than its theoretical estimate. In both iodides the cation (s)+ anion(sp^3) bonding and antibonding states are asymmetrically distributed in energy around the anion p states with some prevalence of the bonding configuration. The anion s states can be found in the BiI_3 XPS curves ~12.3 eV below E_v.[17] The nature of the weak but reproducible peak E' is not clear, although a comparison with the similar PbI_2 EDC's would suggest that it has a spurious origin.

As reported in Table III, only four conduction-band density-of-states peaks, d–g, can be found above the vacuum level VL in the BiI_3 CIS curves. The experiments[4] on the optical transitions from Bi($5d$) to the bottom part of the conduction band show that the similarities between PbI_2 and BiI_3 extend beyond the top of the valence band, since in both materials the lower portion of the conduction band up to the vacuum level exhibits strong cation p character. Therefore, some correlation between the two iodides may be expected even above the VL. For example, the BiI_3 peak d clearly corresponds to peak d of PbI_2. An analysis of the selection rules and of the energy positions indicates that peak g of BiI_3 corresponds to peak i of PbI_2, while the BiI_3 corresponds to a superposition of the PbI_2 peaks g and h although the energy positions in this case do not agree very well.

VI. CONCLUSIONS

The band structure of the layer compounds SnS_2, PbI_2, and BiI_3 has been investigated over a wide energy range employing different synchrotron radiation UPS techniques. The density-of-states peak positions agree with the corresponding theoretical estimates with the exception of the deep-lying valence-band peaks originating from cation s states.

The rather ionic character of the cation-anion bonds in these compounds corresponds to a large contribution of anion p states to the valence band and to a confinement of the cation p states to the conduction band. Some cation s-like contribution is also found in the valence band and its behavior is different in SnS_2 and in the two iodides. In SnS_2 the tin 5s states lie deep in the valence band and do not give any significant contribution to the upper valence band. In PbI_2 and BiI_3 the cation s states combine to some extent with iodine sp^3 hybrids, giving a pair of nonbonding states distributed in bonding and antibonding positions with respect to the energy position of the iodine p states. In all three materials the states at the bottom of the conduction band have marked cation p character, while in the upper regions of the conduction band the atomic orbital character becomes less well defined. In general, more similarities have been found between the electronic structures of PbI_2 and BiI_3 than between these iodides and SnS_2. This confirms the theoretical prediction that the band structure of these materials is much more sensitive to the *chemical properties* of the component atoms than to the crystal lattice structure. The lattice structure is, instead, important in establishing the dif-

ferences between these octahedrally coordinated layer compounds and the layered materials with the GaSe-like structure. For example, the GaSe-like crystals exhibit cation-cation bonds perpendicular to the layers which cannot be found in the CdI_2-like and BiI_3-like crystals. As a consequence, the photon polarization effects in the EDC's are much stronger in the III-VI compounds than in SnS_2, PbI_2, and BiI_3.

The method of employing several different synchrotron radiation photoemission spectroscopy techniques to study the band structure over a wide energy range above and below E_F has already been successfully applied to a large number of materials of different kinds.[1,15] The generally good agreement between the experimental results and theoretical predictions shows that this method is reliable. Therefore, it should be applied in the near future to more complex three-dimensional systems or to other two-dimensional systems such as nonbinary layer compounds, transition-metal dichalcogenides, and ordered adsorbed overlayers.

---

*Postdoctoral Fellow at Bell Laboratories on leave from CNR-GNSM, Rome, Italy.

[1]G. Margaritondo, J. E. Rowe, and S. B. Christman, Phys. Rev. B 15, 3844 (1977).

[2]G. J. Lapeyre, A. D. Baer, J. Hermanson, J. Anderson, J. A. Knapp, and P. L. Gobby, Solid State Commun. 15, 1601 (1974); G. J. Lapeyre, J. Anderson, P. L. Gobby, and J. A. Knapp, Phys. Rev. Lett. 33, 1290 (1975).

[3]G. J. Lapeyre and J. Anderson, Phys. Rev. Lett. 35, 117 (1975).

[4]G. Margaritondo, J. E. Rowe, M. Schlüter, F. Levy, and E. Mooser, Phys. Rev. B 16, 2938 (1977).

[5]C. Y. Fong and M. L. Cohen, Phys. Rev. B 5, 3095 (1972); J. Phys. C 7, 107 (1974); G. Mula and F. Aymerich, Phys. Status Solidi A 51, K35 (1972); E. Mooser, I. Ch. Schlüter, and M. Schlüter, J. Phys. Chem. Solids 35, 1269 (1974); R. B. Murray and R. H. Williams, J. Phys. C 6, 3643 (1973).

[6]G. Margaritondo, J. E. Rowe, M. Schlüter, and H. Kasper, Solid State Commun. 22, 753 (1977).

[7]I. Ch. Schlüter, Phys. Rev. B 9, 1652 (1974).

[8]E. Doni, G. Grosso, and G. Spavieri, Solid State Commun. 11, 493 (1972).

[9]M. Schlüter, M. L. Cohen, S. E. Kohn, and C. Y. Fong, Phys. Status Solidi B 78, 737 (1976).

[10]M. Schlüter and M. L. Cohen, Phys. Rev. B 14, 424 (1976).

[11]J. E. Rowe, G. Margaritondo, H. Kasper, and A. Baldereschi, Solid State Commun. 20, 921 (1976).

[12]The Synchrotron Radiation Center is supported by the NSF under Grant No. DMR-74-15089.

[13]A detailed description of the experimental system is reported in Ref. 1.

[14]J. Camassel, M. Schlüter, J. Kohn, J. P. Voithovsky, Y. R. Shen, and M. L. Cohen, Phys. Status Solidi B 75, 303 (1976).

[15]J. E. Rowe, G. Margaritondo, and S. B. Christman, Phys. Rev. B 16, 1581 (1977).

[16]P. K. Larsen, S. Chiang, and N. V. Smith, Phys. Rev. B 15, 3200 (1977).

[17]G. Margaritondo, J. E. Rowe, M. Schlüter, G. Wertheim, F. Levy, and E. Mooser, Phys. Rev. B 16, 2934 (1977).